Lunar Surface Charging and Electrostatic Lofting of Lunar Dust Particles under Different Solar Wind Conditions and Solar Ultraviolet Radiation

Necmi Cihan Örger*, J. Rodrigo Cordova-Alarcon, Kazuhiro Toyoda, Mengu Cho

Laboratory of Spacecraft Environment Interaction Engineering, Kyushu Institute of Technology, 1-1 Sensui-cho, Tobata-ku, Kitakyushu-shi, Fukuoka, Japan 804-8550, p595502j@mail.kyutech.jp, p595903r@mail.kyutech.jp, toyoda@ele.kyutech.ac.jp, cho@ele.kyutech.ac.jp

* Corresponding Author

Abstract

Lunar surface is electrically charged by continuous flux of ambient plasma as well as exposure to solar radiation. As the Moon orbits the Earth, its plasma environment varies according to its location with respect to the Earth and the Sun. Lunar surface charging is dependent on the electric current sources such as photoemission of electrons by solar irradiation, the collection of electrons and ions from ambient plasma and the secondary emission of electrons from the surface. These current sources can be used to determine the surface potential and electric field, and these values can be highly variable as the current sources alter with time. It has been suggested that lunar horizon glow is produced by forward scattering of the sunlight by electrically charged dust grains that are lofted above the lunar terminator; however, there are significant uncertainties about its physical mechanism. Even though previous laboratory experiments have suggested that intermediate size particles are easier to be lofted from surface by electrostatic forces, the observations of Apollo and Surveyor missions pointed out that smaller size particles in micron to submicron range were responsible for this phenomenon. In our work, various conditions are investigated to find out how surface potential, electric field and Debye length are altered with different parameters. First, it has been seen that subsolar point surface potential is significantly depending on photoemission electrons and solar wind electron current. Second, terminator region surface potential is highly depending on solar wind electron current and, in some cases, ion current. Third, a solar flare event produces strong electric field on subsolar point since most of the photoelectrons are trapped above the positively charged surface. In addition, these results showed that zero potential occurs between subsolar point and terminator region as it is expected, and its location is determined by the photoelectron emission and ambient electron current to the surface dominantly. For these reasons, fast and slow solar wind conditions as well as CME passage on 1-3 May 1998 have been investigated in order to understand nominal and extreme conditions. According to these results, laboratory experiments will be performed in order to understand the electrostatic forces on dust particles and the conditions to launch these particles from the surface. Relative to this work, a CubeSat mission is currently being developed in Kyushu Institute of Technology to observe lunar horizon glow.

Keywords: Lunar dust, lunar surface charging, dust lofting, solar wind, coronal mass ejection.

1. Introduction

As the Moon orbits around the Earth, it directly interacts with ambient plasma since it has neither a global magnetic field nor a dense atmosphere. Ambient plasma conditions vary through the Earth's magnetotail to the solar wind, and lunar surface is charged to an electric potential that reduces the total electric current to the minimum level as any other object in plasma [1].

The Moon receives solar irradiation continuously from the Sun while the fluxes of the solar wind ions and electrons reach the lunar surface directly. Since the electron mass is significantly smaller than ions', most objects in a surrounding plasma tend to be negatively charged in certain conditions; however, the solar irradiation provides photoemission of electrons from the dayside of the Moon due to UV and X-rays. Therefore, the dominance of the photoemission current generates positively charged surface potential on the Moon.

Potential values of approximately +10 V on the dayside and -38 V on the terminator region were reported by Manka under average solar wind conditions [2]. In addition, positively charged dayside region had been predicted before the Apollo missions [3]. Data analysis from Apollo missions showed that the lunar surface was charged positively to approximately +10 V under the solar wind while near terminator and night side regions were charged to approximately -100 V [4]. According to Stubbs et al., these theoretical model predictions are roughly in agreement with observations [5].

Lunar surface charging has several implications, and one of them is electrostatic dust transportation, which has been suspected to be the reason of lunar horizon glow (LHG). LHG was first spotted by onboard TV cameras during Surveyor missions in 1966 and 1968, and it was significantly brighter than the levels that can be supported by micrometeorite ejecta [6]. These observations were related to the lunar terminator, and it has been proposed that LHG was produced by levitated or lofted charged dust grains by electric field above the terminator region.

LHG was also reported by Apollo astronauts [7], and it has been seen as the evidence of the exospheric dust cloud around the Moon over the years; however, the physical mechanism behind the existence of dust grains

in the higher altitudes of lunar exosphere is still being investigated. Even though Apollo 15 and 17 image sequences presented excessive brightness in coronal and zodiacal light (CZL) from another source, Apollo 16 observations exhibited no additional brightness during orbital sunrise [7]. Therefore, LHG can be described as a variable phenomenon, and additional observations or non-observations will provide more evidence of the mechanism behind this excessive brightness and the exospheric dust abundance. The dust cloud and lunar surface potential are presented in Figure 01 below.

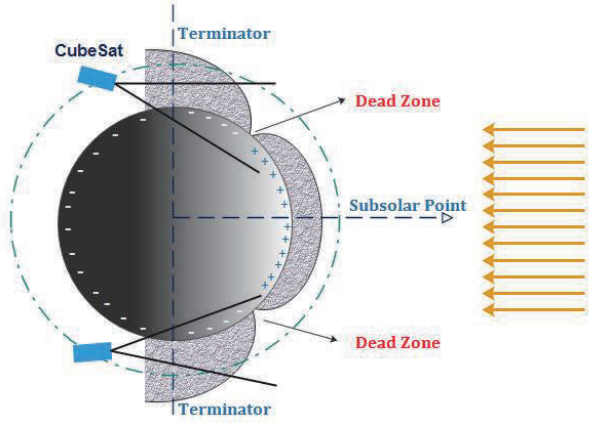

Fig. 1. Lunar Surface Charging and Lofted Dust Cloud.

2. Lunar Surface Charging

Lunar surface charging is dependent on the electric current sources such as photoemission of electrons by solar irradiation, the collection of electrons and ions from ambient plasma and the secondary emission of electrons from the surface [5]. These current sources can be used to determine the surface potential and electric field, and they can be highly variable as the current sources alter with time. In addition to the solar wind the plasma environment is variable when the Moon passes through the geomagnetic tail. The location of the tail depends on the solar activity; therefore, the lunar surface can receive plasma currents from the tail lobes and plasma sheet as well. Even though magnetosheath plasma is similar to the solar wind, charged particles in plasma sheet have higher temperatures and a lower particle density. In this work, the plasma parameters are selected from solar wind conditions, and the geomagnetic tail will be investigated in the future.

2.1 Surface Charging Model

In developing our simulation environment a similar approach has been taken as previous models. Solar wind bulk velocity and the effects of plasma temperature as well as solar irradiance are included to observe the effects of different parameters. It is being developed to include the position of the Sun, Moon and Earth as well as the results from the attitude and orbit control simulations for CubeSat mission to observe the LHG. In this paper, only the results from the lunar surface charging and dust lofting will be presented.

The following equations are solved with the assumptions which are listed below as:

- The Moon is a perfect sphere.
- The interaction with the current sources is in the equilibrium state.
- The lunar surface material conductivity is almost zero.
- Plasma sheath is collisionless.
- The secondary electron emission is negligible.
- Plasma population in the vicinity of the Moon has Maxwellian velocity distribution.
- All ions are protons, and the plasma has no magnetic field.
- Potential distributions in the plasma sheath are monotonic.

In steady state, the net equilibrium current to the surface can be given as:

$$J_{Pe} + J_i + J_e + J_{sec} = 0 \qquad (1)$$

By using this equation the surface potential $\emptyset_s$ can be calculated according to the surrounding plasma conditions and solar irradiation. The elements of this equation can be described as the photoemission electron current J_{Pe}, ion collection current from surrounding plasma J_i, electron collection current from surrounding plasma J_e and the secondary electron emission J_{sec}.

The current equations are dependent on the sign of the surface potential since it will repel or attract different charged particle species.

2.1.1 Positively Charged Surfaces on the Dayside

Positively charged surface on the dayside repel the ion current, whereas the ambient plasma electrons accelerate towards the lunar surface; however, the electron current remains constant since its density will decrease accordingly. In addition, the photoemission current charge the lunar surface positively. When the solar irradiance increases, highly charged lunar surface can attract higher rates of photoelectron population, which creates a dense plasma shield above the surface.

$$J_e = -\frac{n_0 e v_{t_e}}{2\sqrt{\pi}}\left[e^{-{U_e}^2} + U_e\sqrt{\pi}(1+\mathrm{erf}(U_e))\right] \qquad (2)$$

$$J_i = \frac{n_0 e v_{t_i}}{2\sqrt{\pi}}\left[e^{-{X_i}^2} + \frac{V_{bulk}\,cos\theta\sqrt{\pi}}{v_{t_i}}(1+\mathrm{erf}(X_i))\right] \qquad (3)$$

$$J_{Pe} = -e\,n_{Pe0}\sqrt{\frac{k_B T_{Pe}}{2\pi m_e}}\,exp\left\{-\frac{|e\emptyset_s|}{k_B T_{Pe}}\right\}cos\theta \qquad (4)$$

$$J_{sec} = [J_e\delta_e + J_i\delta_i]\exp\left\{-\frac{|e\emptyset_s|}{k_B T_{sec}}\right\} \qquad (5)$$

The local surface potential $\emptyset_s$, the average thermal velocity of the given particle species v_{t_s}, the ambient plasma density n_0, the plasma bulk velocity V_{bulk}, photoelectron density at the lunar surface n_{Pe0}, the solar zenith angle θ, the ratio of plasma bulk velocity to the average thermal velocity as a function of solar zenith angle and the local surface potential X_i and U_e, the secondary electron coefficients for primary particle species $\delta_{e,i}$ are used to determine the current equations as previously given by Manka [2].

2.1.2 Negatively Charged Surfaces on the Dayside and Terminator

Approaching the terminator region leads to drop in the photoemission electron current rapidly since the solar zenith angle reaches 90 degrees. For this reason, it starts to decrease into the levels of electron current from the ambient plasma, and a negative surface potential is expected near the lunar terminator. In addition, the electron current to the surface can overcome positively charging current sources such as ion current and photoemission electron current before reaching the terminator region. Since all photoemission electrons are repelled by negatively charged surfaces or no photoemission occurs due to solar zenith angle, the plasma sheath above the lunar surface is produced by ambient plasma electrons.

$$J_e = -\frac{n_0 e v_{t_e}}{2\sqrt{\pi}}\left[e^{-{X_e}^2} + U_e\sqrt{\pi}(1+\mathrm{erf}(X_e))\right] \quad (6)$$

$$J_i = \frac{n_0 e V_{bulk}\cos\theta}{2}\left[1+\mathrm{erf}(U_i)+\frac{1}{U_i\sqrt{\pi}}e^{-{U_i}^2}\right] \quad (7)$$

$$J_{Pe} = -e\, n_{Pe0}\sqrt{\frac{k_B T_{Pe}}{2\pi m_e}}\ \cos\theta \quad (8)$$

$$J_{sec} = [I_e\delta_e + I_i\delta_i] \quad (9)$$

2.1.3 Dead Zone Location

A transition point between positively charged and negatively charged surfaces on the dayside of the Moon was referred as the "Dead Zone" by Stubbs et al. [8]. Therefore, it is important to determine the location of this zone since the probe equations will be adjusted for the repulsive surfaces to ambient plasma electrons and photoemission electrons.

An analytical solution has been proposed by Stubbs et al. [5] as:

$$\theta_{DZ} = \cos^{-1}\left(-\frac{e n_0}{J_{p0}}\sqrt{\frac{k_B T_e}{2\pi m_e}}\right) \quad (10)$$

This equation was derived from two-current problem, $J_{Pe} + J_e = 0$; however, three-current problem will emerge when the solar wind bulk velocity is very high or the plasma electrons are very cold. For instance, during storm events such as coronal mass ejections (CMEs), the plasma bulk velocity can increase to very high levels while the average electron temperature can be very low. In addition, the secondary electron emission current will become more significant when the Moon traverses in the geomagnetic tail. For these reasons, another equation is proposed in this work as:

$$\theta_{DZ} = \cos^{-1}\left(\frac{n_0\left[\sqrt{T_e/m_e}(1-\delta_e)-\sqrt{T_i/m_i}(1+\delta_i)\right]}{n_{p0}\sqrt{T_{Pe}/m_e}}\right) \quad (11)$$

3. The Surface Charging Results

3.1 Slow Stream Solar Wind

Slow stream solar wind condition has higher plasma density, colder ion temperature and lower solar wind bulk velocity.

Table 1. Slow Stream Solar Wind Conditions [5, 9].

Parameters	Values
Plasma electron density (#/cm$^{3)}$	10.0
Plasma electron temperature (eV)	12.1
Plasma ion temperature (eV)	8.6
Solar wind flow velocity (km s^{-1})	400
Photoelectron current (A m^{-2})	-4.5 x 10^{-6}

Table 2. The Results for Slow Stream Solar Wind.

Regions	**Parameter**	**Value**
Subsolar Point	Surface Potential (V)	+4.2674
(θ=0^o)	Debye Length (m)	1.0282
	Electric Field (V/m)	+4.1503
Intermediate	Surface Potential (V)	+3.2590
region (θ=45^o)	Debye Length (m)	1.2188
	Electric Field (V/m)	+2.6740
Terminator	Surface Potential (V)	-47.5341
(θ=90^o)	Debye Length (m)	8.1773
	Electric Field (V/m)	-5.8129
Dead Zone	Solar Zenith Angle (^{o})	78.8312

The photoemission electron current and the plasma electron current are the dominant sources for surface charging as well as altering the location of the dead zone. Dead zone location moves to lower solar zenith angles since higher density tends to move the dead zone closer to the subsolar point. Positive potential accelerates the plasma electrons approaching to the lunar surface, whereas the photoemission electrons are trapped near the surface. For these reasons, solar wind electron current has a controlling effect of the trapping of photoemission

electrons. While the plasma sheath above the surface is dominated by the photoelectron emission for positive surface potential, photoelectron sheath disappears when the surface potential alters from positive to negative (Fig. 2). In most cases, plasma electron temperature is the most effective parameter since the thermal velocity is the most dominant for electrons.

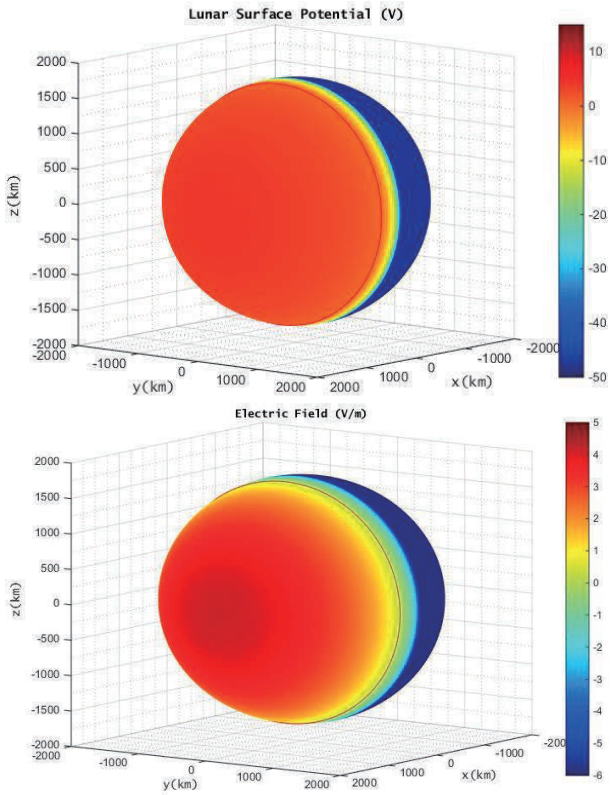

Fig. 2. Lunar Surface Potential (top), Electric Field (bottom) and Dead Zone (Red Line) under Slow Stream Solar Wind.

3.2 Fast Stream Solar Wind

Fast stream solar wind plasma has higher bulk velocity. On the other hand, it has a lower particle density than slow stream. Therefore, the dead zone location is expected to be closer to the terminator region with similar plasma temperature (Fig. 3). The positive surface potential accelerates the plasma electrons, whereas the photoemission electrons are trapped by it.

Table 3. Fast Stream Solar Wind Conditions [5, 9].

Parameters	Values
Plasma electron density (#/cm$^{3)}$	5.0
Plasma electron temperature (eV)	12.1
Plasma ion temperature (eV)	12.9
Solar wind flow velocity (km s^{-1})	650
Photoelectron current (A m^{-2})	-4.5 x 10^{-6}

Table 4. The Results for Fast Stream Solar Wind.

Regions	**Parameter**	**Value**
Subsolar Point (θ=0º)	Surface Potential (V)	+6.3466
	Debye Length (m)	1.0323
	Electric Field (V/m)	+6.1479
Intermediate region (θ=45º)	Surface Potential (V)	+ 5.1583
	Debye Length (m)	1.2256
	Electric Field (V/m)	+4.2088
Terminator (θ=90º)	Surface Potential (V)	-45.0810
	Debye Length (m)	11.5645
	Electric Field (V/m)	-3.8982
Dead Zone	Solar Zenith Angle (º)	84.3789

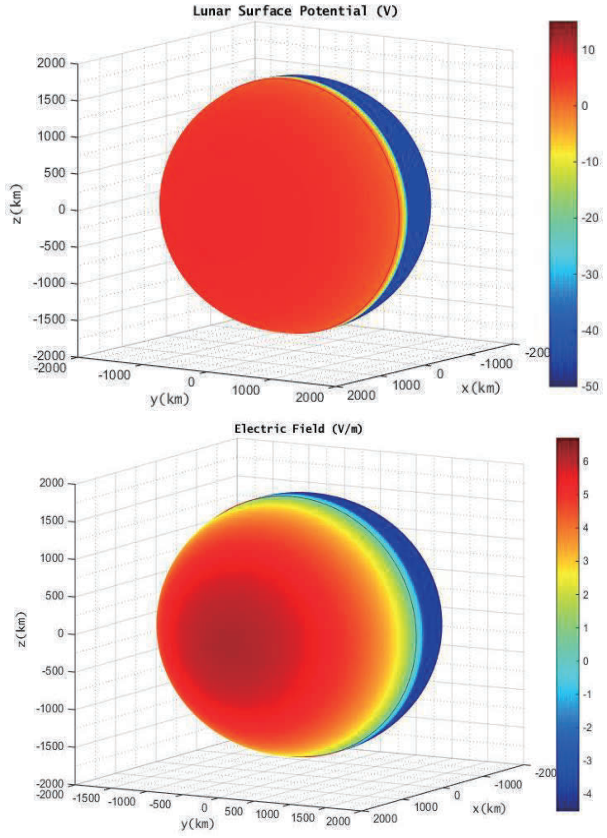

Fig. 3. Lunar Surface Potential (top), Electric Field (bottom) and Dead Zone (Red Line) under Fast Stream Solar Wind.

3.3 CME Post-Shock Plasma

A CME event had occurred from 1 to 3 May 1998 [10], and this event was considered as geo-effective [11]. The lunar plasma environment changes significantly during CME passage; therefore, the lunar surface charge varies accordingly. Following the nominal solar wind, the plasma density, temperature and the bulk velocity start to increase. For instance, the density increases approximately four times of the nominal solar wind.

Therefore, the ambient plasma can be considered as dense and warm.

Table 5. CME Post-Shock Plasma Conditions [10, 11].

Parameters	Values
Plasma electron density (#/cm$^{3)}$	20.0
Plasma electron temperature (eV)	14.8
Plasma ion temperature (eV)	43
Solar wind flow velocity (km s^{-1})	600
Photoelectron current (A m^{-2})	-4.5 x 10^{-6}

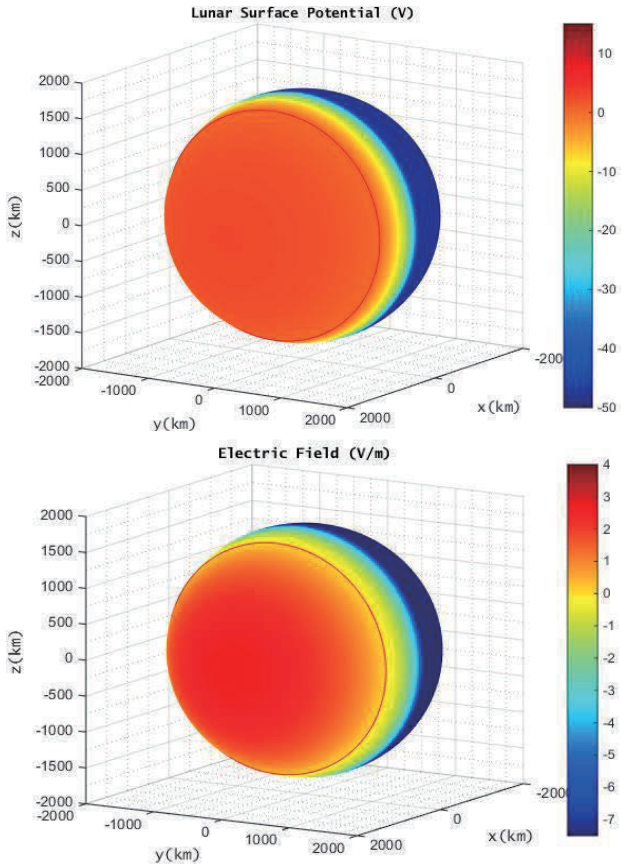

Fig. 4. Lunar Surface Potential (top), Electric Field (bottom) and Dead Zone (Red Line) under CME Post-Shock Plasma.

Since the electron temperature and density increase, subsolar point surface potential decreases, and the dead zone location moves closer to the subsolar point (Fig. 4). High density and temperature creates a stronger electric field at the terminator region since the lunar surface potential is more negative and higher density can create a thinner plasma sheath populated by dense electrons.

Table 6. The Results for CME Post-Shock Region.

Regions	**Parameter**	**Value**
Subsolar Point (θ=0^o)	Surface Potential (V)	+2.8319
	Debye Length (m)	1.0231
	Electric Field (V/m)	+2.7679
Intermediate region (θ=45^o)	Surface Potential (V)	+1.7235
	Debye Length (m)	1.2103
	Electric Field (V/m)	+1.4241
Terminator (θ=90^o)	Surface Potential (V)	-47.7215
	Debye Length (m)	6.3949
	Electric Field (V/m)	-7.4624
Dead Zone	Solar Zenith Angle (^{o})	67.5767

3.4 Early CME Conditions

The incoming plasma is very similar to the nominal solar wind conditions; however, there is an increase in solar irradiation since a solar flare event had occurred [11]. Therefore, the dayside of the Moon has higher photoelectron current in this case, and the inputs are given to the model accordingly (Table 7).

Table 7. Early CME Plasma Conditions [10, 11].

Parameters	Values
Plasma electron density (#/cm$^{3)}$	3.0
Plasma electron temperature (eV)	6.6
Plasma ion temperature (eV)	6.8
Solar wind flow velocity (km s^{-1})	650
Photoelectron current (A m^{-2})	-40 x 10^{-6}

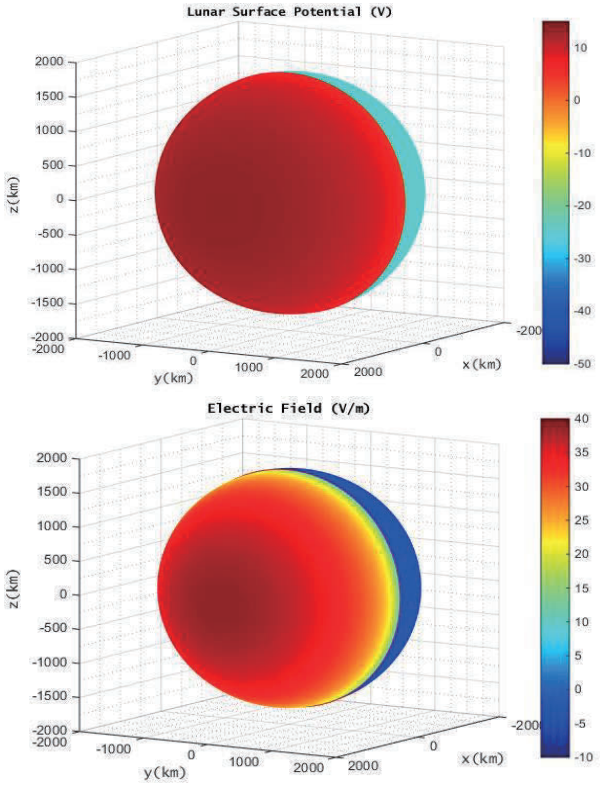

Fig. 5. Lunar Surface Potential (top), Electric Field (bottom) and Dead Zone (Red Line) during Early CME.

Table 8. The Results for Early CME Conditions.

Regions	Parameter	Value
Subsolar Point (θ=0°)	Surface Potential (V)	+13,4906
	Debye Length (m)	0,3475
	Electric Field (V/m)	+38,8262
Intermediate region (θ=45°)	Surface Potential (V)	+12,1178
	Debye Length (m)	0,4131
	Electric Field (V/m)	+29,3327
Terminator (θ=90°)	Surface Potential (V)	-24,7024
	Debye Length (m)	11.0263
	Electric Field (V/m)	-2.2403
Dead Zone	Solar Zenith Angle (°)	89.7111

In this case stronger positively charged surface potential on the dayside is present, and the surface trapping of photoelectrons is expected to be more significant (Fig. 5). Since the Debye length is smaller and the surface potential is stronger, the electric field strength at the subsolar point reaches its maximum value. It can loft the dust grains to higher altitudes on the dayside. On the other hand, the low density and thermal energy of upstream electrons creates a weaker negative potential on the terminator region. Therefore, it is expected that the electrostatic dust transportation is lower at the terminator region in this case. In addition, higher velocity of the solar wind makes the ion current contribute to the positive charging on the dayside.

3.5 Late CME Conditions

During late CME passage, solar wind density becomes higher than all other conditions. On the other hand, the plasma temperature decreases significantly. Therefore, the plasma conditions can be described as highly dense and cold (Table 9).

Table 9. Late CME Plasma Conditions [10, 11].

Parameters	Values
Plasma electron density (#/cm^{3})	50.0
Plasma electron temperature (eV)	3.2
Plasma ion temperature (eV)	2.6
Solar wind flow velocity (km s^{-1})	500
Photoelectron current (A m^{-2})	-4.5 x 10^{-6}

Similar to CME post-shock plasma case, the dead zone moves closer to the subsolar point. First, the relatively high density and temperature of the CME post-shock moves the dead zone location closer to the subsolar point by increasing the electron current to the surface. On the other hand, very high density of late CME tends to increase the electron current whereas the low plasma temperature limits its contribution. Hence, the dead zone ends in a similar location as the CME post-shock plasma case (Fig. 6).

Table 10. The Results for Late CME Conditions.

Regions	Parameter	Value
Subsolar Point (θ=0°)	Surface Potential (V)	+3,5201
	Debye Length (m)	0,9077
	Electric Field (V/m)	+3,8779
Intermediate region (θ=45°)	Surface Potential (V)	+2,0681
	Debye Length (m)	1.0309
	Electric Field (V/m)	+2.0062
Terminator (θ=90°)	Surface Potential (V)	-12.3569
	Debye Length (m)	1.8807
	Electric Field (V/m)	-6.5705
Dead Zone	Solar Zenith Angle (°)	67.6354

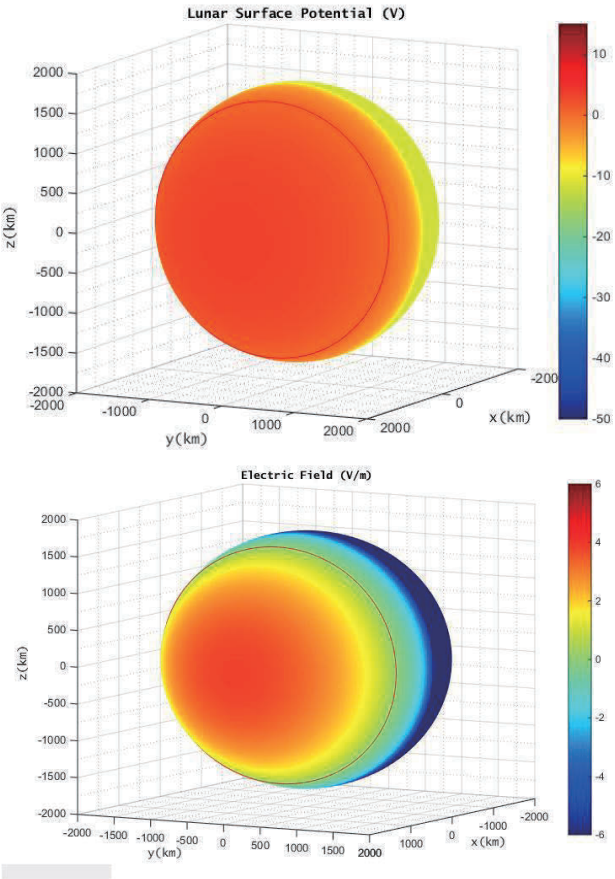

Fig. 6. Lunar Surface Potential (top), Electric Field (bottom) and Dead Zone (Red Line) during late CME.

4. Electrostatic Lunar Dust Transportation

It is suspected that a dust cloud above the lunar surface is present, and LHG is one of the most important evidences. Understanding this fundamental physical process of the lunar environment will improve our

understanding of the Moon, especially the characterization of lunar exosphere. For this reason, it is significantly important to understand the behavior of the dust particles in different conditions. During this study, the results from the lunar surface charging model will be used in lunar dust lofting estimation to further our understanding of this phenomena. In addition, these results will help us to understand light scattering mechanism by dust particles in the exosphere of the Moon, which can point out some of the requirements for the imaging system of our CubeSat mission. Since the observations by Apollo Astronauts was at ~100 km altitude, our objective is to explain these observations based on the particle populations, especially ~0.1 μm dust grains above terminator region.

4.1 Dust Lofting Model

Stubbs et al. (2006) presented Dynamic Fountain Model for lunar dust to explain the existence of high altitude dust grains. According to this method, the net force on a moving dust grain is the subtraction of gravity force and electrostatic force after it leaves the surface since it does not receive the lunar soil cohesion force afterwards [8].

The charge of a dust grain has been given as:

$$q = C\emptyset_s \quad (12)$$

$$C \approx 4\pi\varepsilon_0 r_d \quad (13)$$

The dust grains are accelerate in sheath region above the surface; therefore, they have an exit velocity to reach maximum height while they are decelerating by the influence of lunar gravity. The maximum height h_{max}, time required to reach the maximum height t_{max} and the maximum radius of dust particles that can be lofted r_{max} can be calculated by this model [8].

$$h_{max} = \frac{3\varepsilon_0 \emptyset_s^2}{\rho g_{Lunar} r_d^2} \quad (14)$$

Dust grain mass density ρ, vacuum permittivity ε_0, dust grain radius r_d and lunar gravity g_{Lunar} are used in this equation. The maximum height calculations are given for each case in Table 11.

5. Discussion

Subsolar point surface charging and dust height calculations show that:

- The surface potential is driven by both photoemission electron current and solar wind electron current dominantly.
- Solar wind bulk velocity influences ion current to the surface more than the electron current since the mass of ions are higher than the electrons. Even though plasma bulk velocity has its maximum effect on the subsolar point, the influence of ion current is more distinguishable with extreme values.
- Low density of solar wind plasma decreases the electron current to the lunar surface. Therefore, the surface can be charged to stronger positive potentials, and it attracts higher energy of photoelectrons above the subsolar point. Since the plasma sheath on the dayside is created by photoemission electrons, the lunar surface can be shielded by a thinner plasma sheath by a higher density of emitted electrons. Therefore, the electric field, which charged dust grains are accelerated in, is stronger.
- Warm and dense solar wind plasma decreases the surface potential by higher electron current to the lunar surface; therefore, the electric field is weaker on the

Table 11. Comparison of Dust Height Results.

	Slow Stream SW	*Fast Stream SW*	*CME Post-Shock*	*Early CME*	*Late CME*
Properties	Higher density Lower V_{sw}	Lower Density Higher V_{sw}	High Density Warm Plasma High V_{sw}	Minimum Density Cold Plasma High V_{sw} Maximum J_{pe} (Flare)	Maximum density Minimum Temperature
Maximum Dust Heights					
Terminator					
0.01(μm)	124.84 km	112.29 km	125.83 km	33.72 km	8.44 km
0.1(μm)	1.25 km	1.12 km	1.26 km	0.34 km	0. 09 km
1(μm)	12.48 m	11.23 m	12.58 m	3.37 m	0.84 m
Subsolar Point					
0.01(μm)	1 km	2.23 km	0.44 km	10.01 km	0.68 km
0.1(μm)	10.06 m	22.25 m	4.43 m	100.56 m	6.84 m
1(μm)	0.10 m	0.22 m	0.04 m	1.01 m	0.07 m

subsolar point. During the CME post-shock passage, the dust heights are minimized.

- During a solar flare event, high solar irradiance increases the photoemission electron density above the surface. In addition, the solar wind density has its minimum level during early CME; therefore, the subsolar surface potential reaches its maximum positive value by both high photoemission current from the surface and low electron current to the lunar surface. This positive potential attracts ambient electrons stronger as well as the photoemission electrons; therefore, most of the photoemission electrons are trapped above the positively charged surface. It creates a dense and thin plasma sheath, and Debye length has its minimum value during this event. For this reason, the electric field is stronger on the dayside. Therefore, the dust heights have their maximum value on the dayside during a flare event. It is ~5 times higher than regular solar wind conditions.
- During the late CME passage, the plasma density has its maximum value, and it tends to increase the electron current to the surface. On the other hand, the electron current is driven mostly by electron temperature; therefore, cold plasma temperature decreases the electron current more than the contribution of high density.
- Even though the plasma properties of post-shock and late CME are different, they produce similar effects on the dust transportation at the subsolar point, where the maximum dust heights are lower than other cases.

Terminator region surface charging and dust height calculations show that:

- It is driven by both solar wind electron and ion currents, and the electron current dominates the surface charging whereas the photoemission current disappears.
- Debye shield is created by solar wind electrons, which is different than the subsolar point case.
- Low density of solar wind plasma decreases the electron current. Therefore, the surface is charged to weaker negative potentials; however, the influence of the electron temperature is more significant.
- Slow and fast stream solar wind produce negative surface potentials with closer values; however, high density of slow stream produces a thinner Debye shield above the terminator region. Therefore, the electric field is stronger than the fast stream case. For this reason, the dust heights are higher during slower streams even though the difference is not significant.
- During the CME post-shock passage, warm and dense plasma produces a strong electric field, which results from thinner Debye shield and high negative surface potential. Therefore, the dust heights are maximum during this interval.
- Similar to the influence of solar wind flow bulk velocity, photoemission current disappears while reaching the terminator region. Therefore, a solar flare event does not influence the dust transportation above the terminator region.
- Solar wind density has its minimum level during late CME passage; therefore, Debye shield is considerably thicker than late CME case, and low density accompanied by low electron temperature produces weaker negative surface potential. Therefore, the dust heights have lower values than the most cases.
- During the late CME passage, the plasma temperature is minimum; therefore, the surface potential is also minimized. On the other hand, the maximum value of particle density creates a very thin Debye shield; therefore, it produces a strong electric field; however, the dust particles are charged to weak potentials similar to the surface. For this reason, they cannot be accelerated to high altitudes in this electric field. Therefore, the dust heights are minimum in this case.

6. Conclusions

In this study, various plasma conditions are investigated in order to calculate lunar surface potential, electric field, Debye length and maximum dust heights from the subsolar point to terminator region. In addition, these results showed that there is a location where the heights of lofted dust grains are minimum between subsolar point and terminator region as it is expected, and its position changes according to the solar wind properties and photoemission electron current. For this purpose, another equation has been proposed for calculating the Dead Zone location.

Previous studies and experiments showed that cohesion force significantly influences small size dust particles [12, 13]. Therefore, it is expected that intermediate size particles can be lofted from the lunar surface initially since they receive more currents than smaller particles and become charged earlier. In addition, they receive less cohesive forces.

In the near future, laboratory experiments will be performed in order to improve the dust model by focusing on the electrostatic interaction between charged dust grains in plasma by utilizing the surface charge and electric field results, and the simulation environment will be improved. Relative to this work, a CubeSat mission is currently being planned in Kyushu Institute of Technology to observe LHG.

References

[1] Whipple, E. C. (1981). Potentials of surfaces in space. *Reports on Progress in Physics*, *44*(11), 1197.

[2] Manka, R. H. (1973). Plasma and potential at the lunar surface. *Photon and Particle Interactions with Surfaces in Space* (pp. 347-361). Springer Netherlands.

[3] Walbridge, E. W. (1969). On "Photoelectric screening of bodies in interplanetary space" by Singer and Walker. *Icarus*, *10*(2), 342-343.

[4] Freeman, J. W., & Ibrahim, M. (1975). Lunar electric fields, surface potential and associated plasma sheaths. *Earth, Moon, and Planets*, *14*(1), 103-114.
[5] Stubbs, T. J., Farrell, W. M., Halekas, J. S., Burchill, J. K., Collier, M. R., Zimmerman, M. I., ... & Pfaff, R. F. (2014). Dependence of lunar surface charging on solar wind plasma conditions and solar irradiation. *Planetary and Space Science*, *90*, 10-27.
[6] Rennilson, J. J., & Criswell, D. R. (1974). Surveyor observations of lunar horizon-glow. *The Moon*, *10*(2), 121-142.
[7] McCoy, J. E. (1976, April). Photometric studies of light scattering above the lunar terminator from Apollo solar corona photography. *Lunar and Planetary Science Conference Proceedings* (Vol. 7, pp. 1087-1112).
[8] Stubbs, T. J., Vondrak, R. R., and Farrell, W. M. (2006). A dynamic fountain model for lunar dust. *Advances in Space Research*, *37*(1), 59-66.
[9] Baumjohann, W., & Treumann, R. A. (1997). *Basic space plasma physics*. World Scientific.
[10] Farrell, W. M., Halekas, J. S., Killen, R. M., Delory, G. T., Gross, N., Bleacher, L. V., ... & Zimmerman, M. I. (2012). Solar-Storm/Lunar Atmosphere Model (SSLAM): An overview of the effort and description of the driving storm environment. Journal *of Geophysical Research: Planets, 117*(E10).
[11] Farrell, W. M., Poppe, A. R., Zimmerman, M. I., Halekas, J. S., Delory, G. T., & Killen, R. M. (2013). The lunar photoelectron sheath: A change in trapping efficiency during a solar storm. Journal o*f Geophysical Research: Planets, 118*(5), 1114-1122.
[12] Hartzell, C. M., Wang, X., Scheeres, D. J., & Horányi, M. (2013). Experimental demonstration of the role of cohesion in electrostatic dust lofting. *Geophysical Research Letters, 40*(6), 1038-1042.
[13] Hartzell, C. M., & Scheeres, D. J. (2011). The role of cohesive forces in particle launching on the Moon and asteroids. *Planetary and Space Science, 59*(14), 1758-1768.